Electric field tunable anisotropic magnetoresistance effect in an epitaxial $Co_2FeSi/BaTiO_3$ interfacial multiferroic system

S. Yamada,[1,2] Y. Teramoto,[2] D. Matsumi,[2] D. Kepaptsoglou,[3,4] I. Azaceta,[4] T. Murata,[2] K. Kudo,[2] V. K. Lazarov,[4] T. Taniyama,[1,5] and K. Hamaya[1,2,*]

[1]*Center for Spintronics Research Network, Graduate School of Engineering Science, Osaka University, Toyonaka, Osaka 560-8531, Japan*

[2]*Department of Systems Innovation, Graduate School of Engineering Science, Osaka University, Toyonaka, Osaka 560-8531, Japan*

[3]*SuperSTEM Laboratory, Daresbury, WA4 4AD, United Kingdom*

[4]*Department of Physics, University of York, York YO10 5DD, United Kingdom*

[5]*Department of Physics, Nagoya University, Chikusa-ku, Nagoya 464-8602, Japan*

(Received 31 March 2020; revised 25 October 2020; accepted 6 January 2021; published 22 January 2021)

We study magnetic and magnetotransport properties of an epitaxial interfacial multiferroic system consisting of a ferromagnetic Heusler-alloy Co_2FeSi and a ferroelectric-oxide $BaTiO_3$. $L2_1$-ordered Co_2FeSi epilayers on $BaTiO_3(001)$ show an in-plane uniaxial magnetic anisotropy with strong temperature dependence, induced by the presence of the magnetoelastic effect via the spin-orbit interaction at the $Co_2FeSi/BaTiO_3(001)$ interface. In the Co_2FeSi Hall-bar devices, the anisotropic magnetoresistance (AMR) hysteretic curves depending on in-plane magnetization reversal processes on the a and c domains of $BaTiO_3(001)$ are clearly observed at room temperature. Notably, the magnitude of the AMR ratio (%) for Co_2FeSi Hall-bar devices can be tuned through the $a-c$ domain wall motion of $BaTiO_3(001)$ by applying electric fields. We propose that the tunable AMR effect is associated with the modulation of the spin-orbit interaction, exchange interaction, and/or the electronic band structure near the Fermi level by applying electric fields in the epitaxial $Co_2FeSi/BaTiO_3(001)$ interfacial multiferroic system.

DOI: 10.1103/PhysRevMaterials.5.014412

I. INTRODUCTION

In the research field of spintronics, electric field control of magnetic properties in ferromagnetic layers has been proposed and demonstrated as a next-generation technology for switching the magnetization orientation with low power consumption in magnetic memories [1–6]. The use of dielectric materials as a gate insulator enables us to modulate electric charges in magnetic materials, leading to a variation in the ferromagnetism [1] and magnetic anisotropy [2–4]. Although different ferroic orders in multiferroic materials such as $TbMnO_3$ and $BiFeO_3$ can be controlled by an electric field [5,6], the magnetic order in these single-phase multiferroic materials is generally antiferromagnetic with a weak coupling among the ferroic orders. Thus, the use of the single-phase multiferroic materials for the electric field control of magnetism is limited to temperatures lower than room temperature [6]. As another promising magnetization control technique by an electric field above room temperature, interfacial multiferroic systems consisting of ferromagnetic (FM) and ferroelectric (FE) materials have been proposed [7–14]. In particular, the magnetoelastic effect via strain transfer across the FM/FE interfaces in conventional FM/perovskitelike FE oxide systems, $Fe/BaTiO_3$ and $CoFe/BaTiO_3$, has been demonstrated above room temperature [15–19]. In the interfacial multiferroic systems, the bonding modulation effect [20], charge modulation effect [21], and magnetoionic effect [22] can also be expected above room temperature.

So far, the FM/FE heterostructures consisting of Co-based Heusler alloys and $BaTiO_3$ have theoretically been examined by first-principles density functional calculations [23–27]. Since it is well known that the Co-based Heusler alloys such as Co_2MnSi and Co_2FeSi are half-metallic materials with high Curie temperatures [28–30], lots of spintronic applications have been explored in magnetic tunnel junctions [31,32] and semiconductor devices [33–36]. If these Co-based Heusler alloys are integrated with FE materials such as $BaTiO_3$, an enhancement in the charge modulation effect is expected [23–27] because the inverse magnetoelectric-effect coefficient is proportional to the spin polarization of the FM materials. However, there is no report on experimental demonstration of the magnetoelectric effect in the interfacial multiferroic systems with Co-based Heusler alloys.

In this paper, we experimentally study magnetic and magnetotransport properties of an interfacial multiferroic system consisting of Co_2FeSi and $BaTiO_3$. For an epitaxial $Co_2FeSi/BaTiO_3$ system, an in-plane uniaxial magnetic anisotropy and its strong temperature dependence, induced by the presence of the magnetoelastic effect via the spin-orbit interaction at the $Co_2FeSi/BaTiO_3(001)$ interface, are seen. By applying electric fields to the epitaxial $Co_2FeSi/BaTiO_3(001)$, the anisotropic magnetoresistance (AMR) effect can be tuned through the $a-c$ domain wall motion of $BaTiO_3(001)$ for Co_2FeSi Hall-bar devices formed on the a and c domains of $BaTiO_3(001)$. We discuss

*hamaya@ee.es.osaka-u.ac.jp

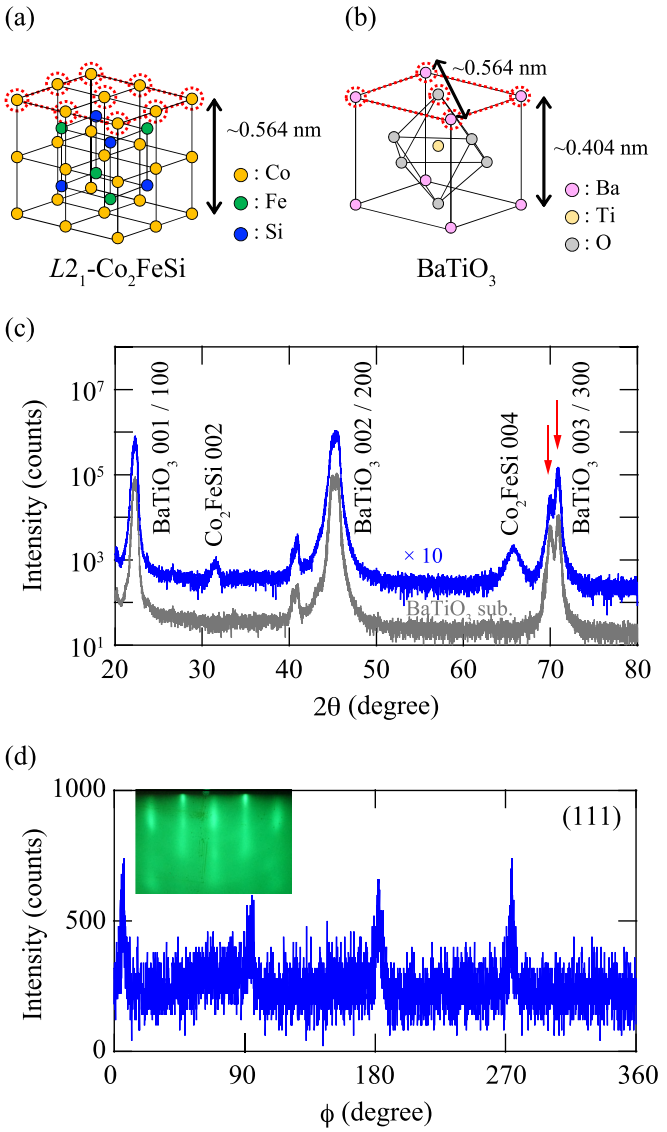

FIG. 1. Schematics of crystal structure and atomic arrangements of (001) plane for (a) Co_2FeSi and (b) $BaTiO_3$, respectively. (c) θ-2θ measurements and (d) ϕ-scan measurements of (111) plane for an MBE-grown Co_2FeSi layer. The gray data in Fig. 1(c) is the θ-2θ XRD pattern for a $BaTiO_3$(001) substrate. The intensity of the θ-2θ XRD pattern for the $Co_2FeSi/BaTiO_3$ heterostructure is multiplied by a factor of 10. The inset in Fig. 1(d) shows a RHEED pattern of the surface after the growth of the Co_2FeSi layer on $BaTiO_3$(001).

possible origins of the tunable AMR effect in the epitaxial $Co_2FeSi/BaTiO_3$(001) interfacial multiferroic system.

II. CRYSTAL STRUCTURES AND CHARACTERIZATIONS

Co_2FeSi epilayers were grown on $BaTiO_3$(001) substrates by molecular beam epitaxy (MBE) at 200 °C [37–39]. Figures 1(a) and 1(b) illustrate the crystal structures and the atomic arrangement of (001) plane for $L2_1$-ordered Co_2FeSi and $BaTiO_3$, respectively. Because the mismatch between the lattice constant of Co_2FeSi (∼0.564 nm) [40,41] and the diagonal length of $BaTiO_3$ ($\sqrt{2} \times 0.399$ nm = 0.564 nm) [12] is less than 0.1%, an epitaxial relationship of Co_2FeSi(001)[100]//$BaTiO_3$(001)[110] can be expected.

In the following, we briefly explain the growth procedure and characterizations for the Co_2FeSi epilayers. After loading a $BaTiO_3$(001) substrate into an MBE chamber, we performed heat treatment at 400 °C for 20 min with a base pressure of $\sim 10^{-7}$ Pa. By *in situ* reflection high-energy electron diffraction (RHEED) observations, good surface flatness of the $BaTiO_3$(001) surface was confirmed (not shown here). Cooling the substrate temperature down to 200 °C, we grew Co_2FeSi layers with thicknesses of 5, 10, and 30 nm by co-evaporating Co, Fe, and Si elements using Knudsen cells [37–39]. After the growth, structural characterizations were conducted by *in situ* RHEED, x-ray diffraction (XRD), high-angle annular dark-field scanning transmission electron microscopy (HAADF-STEM), and energy dispersive x-ray spectroscopy (EDX) measurements.

Magnetic properties were measured by using a vibrating sample magnetometer (VSM) at various temperatures. In this study, we focus on the low-field AMR effect of the $Co_2FeSi/BaTiO_3$ heterostructures, where the longitudinal resistance (R_{xx}) depends on the relative orientation between the magnetization (M) and current flow (I) directions [42]. To explore the AMR effect, the Co_2FeSi layers were patterned into a 80-μm-wide and 400-μm-long Hall-bar shape along $BaTiO_3$ [100] direction using photolithography and wet etching. The AMR measurements were performed by a standard four-point dc method at room temperature under the application of in-plane external magnetic fields (H).

III. RESULTS

A. Structural and magnetic properties

The inset of Fig. 1(d) shows an *in situ* RHEED pattern of a Co_2FeSi layer during the growth. Even for the low growth temperature at 200 °C, we can see the RHEED image with symmetrical streaks indicating two-dimensional epitaxial growth. The θ-2θ XRD pattern for the Co_2FeSi layer is shown in Fig. 1(c) (blue), together with that for a $BaTiO_3$ substrate (gray). 002 and 004 diffraction peaks of Co_2FeSi are clearly observed at 2θ of ∼32° and ∼66°, respectively, ensuring the formation of a (001)-oriented Co_2FeSi epilayer. $BaTiO_3$ substrates used here possess a tetragonal crystal structure at room temperature and a ferroelectric polarization along the c axis [43]. The splitting of $h00$ and $00l$ diffraction peaks of $BaTiO_3$ observed (see red arrows) indicates the coexistence of two types of ferroelectric domains, square c domains and rectanglar a domains, in the $BaTiO_3$ substrates at room temperature [16]. From the ϕ-scan measurements of (202) plane for the Co_2FeSi layer (not shown here), we confirmed the in-plane crystal orientation of Co_2FeSi[100](001)//$BaTiO_3$[110](001). The ϕ-scan measurement of (111) plane is presented in Fig. 1(d). Diffraction peaks with fourfold symmetry are seen, indicating the presence of $L2_1$-ordered structures in the Co_2FeSi layers.

Figure 2(a) displays a typical HAADF-STEM image with EDX line profiles for the epitaxial $Co_2FeSi/BaTiO_3$(001) heterostructure. The contrast of the HAADF-STEM image in the Co_2FeSi epilayer is nearly uniform, indicating the absence

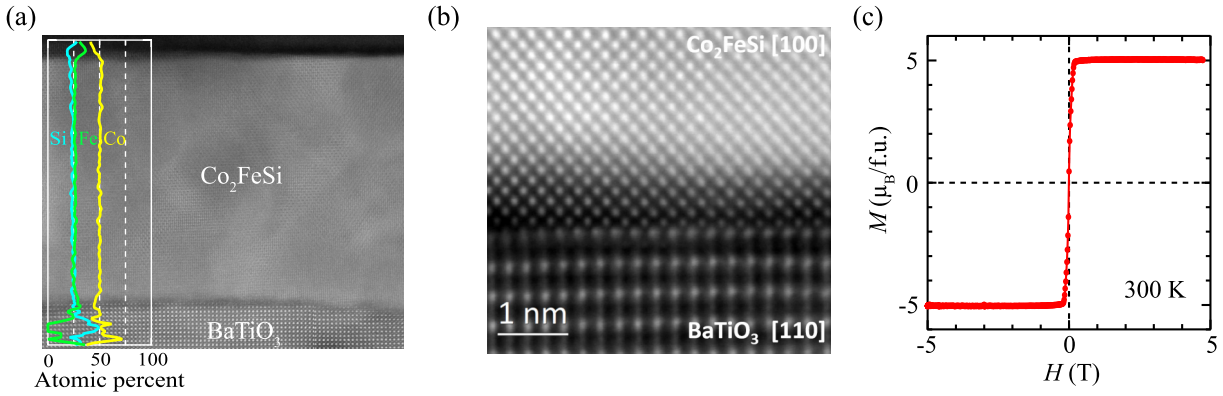

FIG. 2. (a) HAADF-STEM image with EDX line profiles of an epitaxial $Co_2FeSi/BaTiO_3(001)$ heterostructure. (b) Atomic resolution HAADF-STEM image of the $Co_2FeSi/BaTiO_3$ interface, acquired along the $BaTiO_3$ [110] and Co_2FeSi [100] zone axes, respectively, showing the abrupt epitaxial growth of the Co_2FeSi epilayer. (c) A high-field M-H curve at 300 K for the $Co_2FeSi/BaTiO_3$ heterostructure.

of the structural local disorder like inhomogeneous phases. The EDX line profiles of the epitaxial $Co_2FeSi/BaTiO_3(001)$ are also presented in the inset of Fig. 2(a). The chemical composition of the Co_2FeSi epilayer along the layer normal direction is perfectly stoichiometric (Co : Fe : Si = 2 : 1 : 1). From these characterizations, we conclude that the homogeneous and single-phase Co_2FeSi epilayers are obtained by the low-temperature MBE technique [37–39]. Figure 2(b) shows an atomic resolution HAADF-STEM image near the $Co_2FeSi/BaTiO_3$ interface acquired along the $BaTiO_3$ [110] and Co_2FeSi [100] zone axis, respectively, confirming the abrupt epitaxial growth of the Co_2FeSi layer. No secondary phases are observed in the images.

Figure 2(c) shows a high-field magnetization curve (M-H curve) of the Co_2FeSi epilayer on $BaTiO_3(001)$ at 300 K. The value of the saturation magnetic moment (M_S) is estimated to be ~5.1 μ_B/f.u., comparable to that for Co_2FeSi epilayers with a high spin polarization [37,44,45]. From the structural and magnetic characterizations, we regard the grown $Co_2FeSi/BaTiO_3(001)$ heterostructure as an epitaxial ferromagnetic full-Heusler alloy/ferroelectric system.

B. Observation of magnetoelastic effect

$BaTiO_3$ is a typical displacive type ferroelectric material. As shown in the inset of Fig. 3(a), $BaTiO_3$ exhibits the structural phase transitions from the tetragonal to the orthorhombic at ~278 K and from the orthorhombic to the rhombohedral at ~183 K [12,43]. Because the Co_2FeSi layer is epitaxially grown on $BaTiO_3$, the phase transition of $BaTiO_3$ can induce the strain variation in the Co_2FeSi epilayer via the heterointerface at the phase transition temperatures. Figure 3(a) shows the temperature dependence of the magnetization (M-T curve) of a 30-nm-thick $Co_2FeSi/BaTiO_3(001)$ heterostructure under the application of an external magnetic field of 0.5 mT along [100] (blue) and [010] (red) directions of $BaTiO_3$. With decreasing measurement temperature, the magnetization dramatically changes at 275–280 K and slightly changes at 180–185 K, arising from the changes in the lattice strain at the $Co_2FeSi/BaTiO_3(001)$ interface at the phase transitions of $BaTiO_3$, tetragonal to orthorhombic and orthorhombic to rhombohedral. The behavior of such M-T curves is reproducibly observed for other *samples* (not shown here). The magnetic properties clearly indicate the observation of the magnetoelastic effect via the spin-orbit interaction at the interface in the epitaxial $Co_2FeSi/BaTiO_3$ interfacial multiferroic systems.

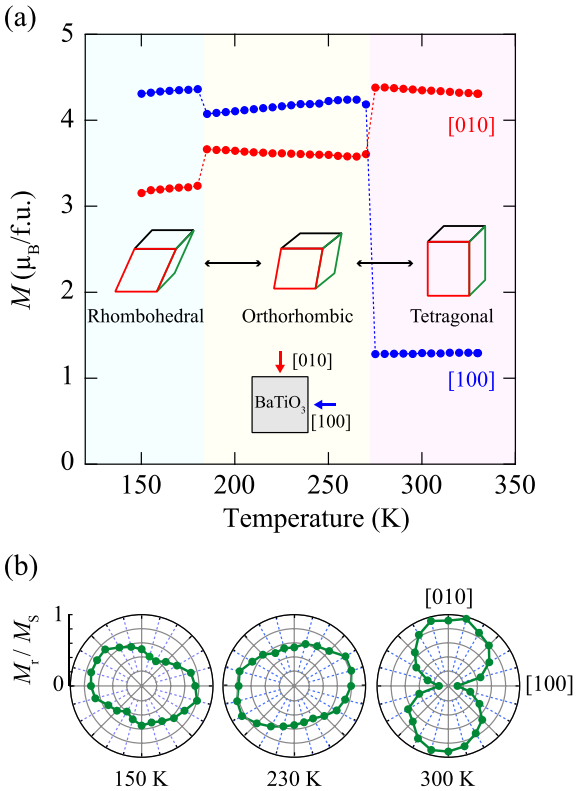

FIG. 3. (a) M-T curves for an epitaxial $Co_2FeSi/BaTiO_3$ heterostructure under the application of an H of 0.5 mT. The directions of H under the measurements are also depicted in the inset. Schematics of structural phase transitions from tetragonal to orthorhombic phases at 278 K and from orthorhombic to rhombohedral phases at 183 K in $BaTiO_3$ are also shown in the inset. (b) Polar plots of the normalized remanent magnetization (M_r/M_s) at 300 K (tetragonal phase), 230 K (orthorhombic phase), and 150 K (rhombohedral phase).

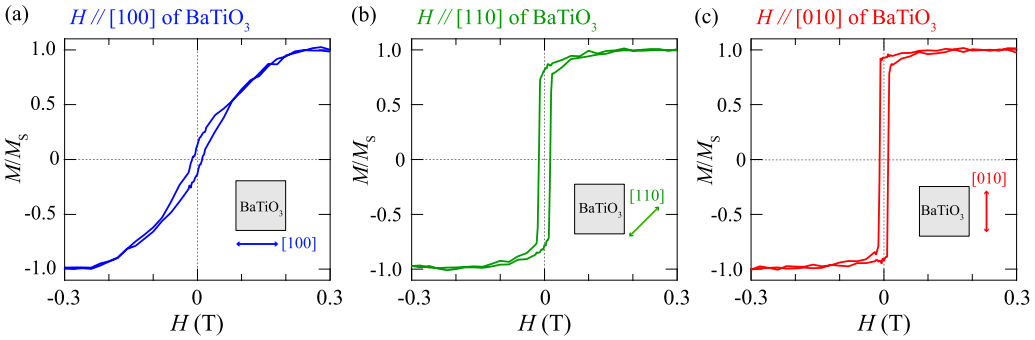

FIG. 4. Low-field M-H curves for an epitaxial $Co_2FeSi/BaTiO_3$ heterostructure, measured under applying H along (a) [100], (b) [110], and (c) [010] directions of $BaTiO_3$ at 300 K.

We also examined low-field M-H curves for different H directions in the layer plane at 150, 230, and 300 K, where each temperature corresponds to the rhombohedral, orthorhombic, and tetragonal phases of $BaTiO_3$, respectively. Here, the samples are rotated in the (001) film plane to change the relative orientation between the H direction and [100] crystallographic axis of $BaTiO_3$. In Fig. 3(b) we plot the remanent magnetization (M_r) normalized by M_S as a function of crystallographic orientation of $BaTiO_3$ at 150, 230, and 300 K. Although the crystal structure of Co_2FeSi has fourfold symmetry in the (001) plane, as illustrated in Fig. 1(a), an in-plane uniaxial magnetic anisotropy can be seen. This feature is largely different from the $Fe/BaTiO_3$ heterostructure reported previously [12,17], where Fe also has a bcc crystal structure like Co_2FeSi. Because of the magnetoelastic effect via the interfacial strain, we regard the magnetic easy axis of the Co_2FeSi epilayers as the same axis along the long axis of the rectangle in the a domain of $BaTiO_3$. Considering the data in Fig. 3(b), we explain again the detailed M-T features in Fig. 3(a). Although a uniaxial magnetic anisotropy is seen at each temperature, large changes in the direction of the magnetic easy axis are observed at both phase transition temperatures (∼278 K and ∼183 K). Also, with decreasing temperature, the strength of the uniaxial magnetic anisotropy becomes small at around 280 K. From these results, we interpret that the magnetization directions of the Co_2FeSi epilayers are mainly affected by the a domains of $BaTiO_3$, enclosed area by red and green lines, respectively, in the inset of Fig. 3(a). It should be noted that the strength of the uniaxial magnetic anisotropy at lower temperatures is relatively small compared to those observed at higher temperatures because the magnetic hard axis is not evident. These magnetic anisotropy changes with thermal perturbation are strong evidence for the achievement of the epitaxial $Co_2FeSi/BaTiO_3$ interfacial multiferroic systems.

To focus on the room-temperature magnetic anisotropy in detail, we further explore the shape of M-H curves for the epitaxial $Co_2FeSi/BaTiO_3$ heterostructures for different H directions. Figure 4 displays in-plane M-H curves measured in H along (a) [100], (b) [110], and (c) [010] directions of $BaTiO_3$ at 300 K for an epitaxial $Co_2FeSi/BaTiO_3(001)$ heterostructure, respectively. Here, the Co_2FeSi layer is the same sample shown in Fig. 3. On the basis of the value of M_r presented in Fig. 3, we should consider a uniaxial easy axis along [010] of $BaTiO_3$ and a uniaxial hard axis along [100] of $BaTiO_3$. However, in the M-H curve measured along [100] of $BaTiO_3$, we clearly observe hysteretic behavior within H between ±0.05 T in Fig. 4(a), which cannot be explained only by a strong uniaxial anisotropy along [010] of $BaTiO_3$. Since it is well known that $BaTiO_3(001)$ has a and c domains divided by 90° domain walls [46–48], we should also take into account an influence of the Co_2FeSi epilayer grown on the c domains of $BaTiO_3$ that gives rise to the cubic magnetocrystalline anisotropy along ⟨110⟩ of $BaTiO_3$. For a thinner Co_2FeSi epilayer, we found that, in the M-H curve along [010] or [110] of $BaTiO_3$, the two-step magnetization switching of the Co_2FeSi epilayers is observed, also indicating the presence of the cubic magnetocrystalline anisotropy along ⟨110⟩ of $BaTiO_3$, as shown in Fig. S1 [49]. Similar two-step switching features were observed in Fe/GaAs(100) [50] and (Ga,Mn)As/GaAs(100) [42,51] with both conventional cubic magnetocrystalline and unconventional uniaxial magnetic anisotropies. Therefore, although it has been indicated that there is a uniaxial anisotropy due to the a domain of the $BaTiO_3$ in the Co_2FeSi epilayers grown on $BaTiO_3(001)$ (Fig. 3), we have to take into account the influence of the conventional cubic magnetocrystalline anisotropy along ⟨110⟩ of $BaTiO_3$, arising from the c domain of the $BaTiO_3$.

C. Electric-field control of AMR effect

A schematic illustration and an optical micrograph of a $Co_2FeSi/BaTiO_3$ Hall-bar device are shown in Figs. 5(a) and 5(b), respectively. In Fig. 5(b) we can see stripe patterns consisting of a and c domains divided by 90° domain walls in $BaTiO_3$ [46–48]. In this study, we have investigated the magnetotransport properties of Co_2FeSi epilayers with three different thicknesses of 5, 10, and 30 nm on $BaTiO_3$ using lots of Hall-bar devices. Since all the devices are fabricated along stripe patterns parallel to the [100] axis of $BaTiO_3$ [Fig. 5(b)], the direction of the current I is also along the same direction. Here, we define the relative orientation ϕ between the directions of I and H, as depicted in Fig. 5(a), and the AMR is measured as a function of ϕ. In the following, the magnetotransport behavior of representative devices with 10-nm-thick Co_2FeSi epilayers are presented.

Figure 5(c) shows a low-field MR curve, $R_{xx}(=\frac{V_{xx}}{I})$ versus H, of a Hall-bar device (named *device* A) at room temperature before applying an electric field (E). Here we measure the MR hysteresis curves after saturating the magnetization along two

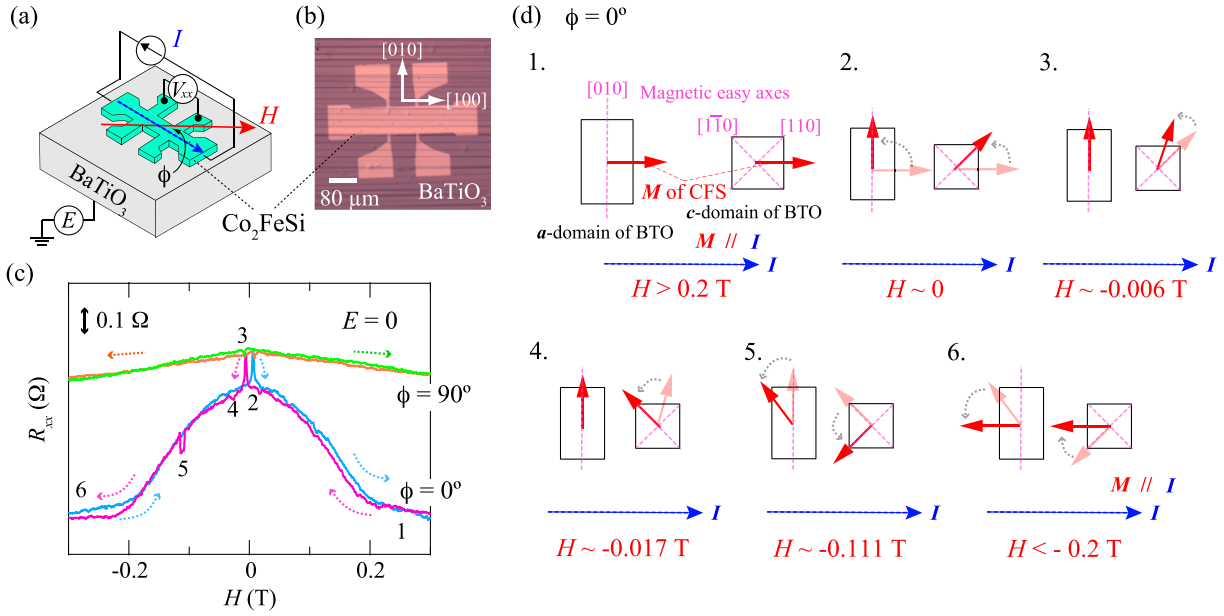

FIG. 5. (a) Schematic and (b) optical micrograph of a fabricated Co_2FeSi Hall-bar device on $BaTiO_3$. (c) Room-temperature R_{xx}-H curves of *device* A for $H//[100]$ of $BaTiO_3$ and $H \perp [100]$ of $BaTiO_3$ at an E of zero. (d) Schematics of the correlation between magnetization directions of the Co_2FeSi epilayer and a or c domain of $BaTiO_3$ under sweeping H. The dotted pink lines correspond to the magnetic easy axis of the Co_2FeSi epilayers on each domain of $BaTiO_3$.

different H directions ($\phi = 0^\circ$ and $\phi = 90^\circ$). Clear hysteresis curves based on the AMR effect of the Co_2FeSi epilayer are reproducibly obtained by sweeping H. To consider the correlation between the magnetization reversal process of Co_2FeSi and the AMR feature, the numbers from 1 to 6 are labeled in the hysteresis data for $\phi = 0^\circ$, as shown in Fig. 5(c). In this data, we first find a bell-shaped curve with respect to H. In addition to this, there are two characteristic changes of R_{xx} around the magnetic fields labeled 3 and 5.

Given these characteristic features, we discuss the detailed in-plane magnetization reversal processes of the Co_2FeSi epilayer on the a and c domains of $BaTiO_3(001)$ for $\phi = 0^\circ$ in Fig. 5(d), where schematics of the magnetization (M) directions of Co_2FeSi are illustrated. First, in a high H regime ($H > 0.2$ T) along $BaTiO_3$ [100] (labeled by 1), the M directions of the Co_2FeSi epilayer on both a and c domains of $BaTiO_3$ are fully aligned along the H ($BaTiO_3$ [100]) direction, leading to the smallest relative orientation between M and I ($M//I$), as shown in 1 of Fig. 5(d). Hence, we detect the smallest resistance value in $H > 0.2$ T. With decreasing H to zero, the value of R_{xx} gradually increases (labeled by 2). This feature can be understood by the change in the M direction of the Co_2FeSi epilayer on the a domain of $BaTiO_3$ to the uniaxial easy axis along $BaTiO_3$ [010] and that of the Co_2FeSi epilayer on the c domain of $BaTiO_3$ to the cubic magnetocrystalline easy axis along $BaTiO_3$ [110], as shown in 2 of Fig. 5(d), because of the influence of the anisotropy fields. After reversing the H direction and decreasing H to ~ -0.006 T, the value of R_{xx} reaches the maximum value (labeled by 3). This means that the M directions of the Co_2FeSi epilayer on both a and c domains of $BaTiO_3$ are nearly aligned to the $BaTiO_3$ [010] direction, indicating the largest relative orientation between M and I, as shown in 3 of Fig. 5(d). At $H \sim -0.017$ T, the value of R_{xx} suddenly decreases (labeled by 4) due to a reduction in the relative orientation between M and I. This feature implies that only the M direction of the Co_2FeSi epilayer on the c domain of $BaTiO_3$ is varied to an easy axis, as shown in 4 of Fig. 5(d). With a further decrease in H, resistance changes are seen at $H \sim -0.111$ T. Because of the presence of a small misalignment between H and I, the magnetization reversal processes shown in 5 of Fig. 5(d) are expected. Finally, in $H < -0.2$ T, the M of the Co_2FeSi layer is fully aligned again to the H ($BaTiO_3$ [$\bar{1}$00]) direction, giving rise to the smallest relative orientation between M and I ($M//I$), as shown in 6 of Fig. 5(d). From these considerations, we can qualitatively understand the low-field MR features as consequences of the in-plane magnetization reversal processes of the Co_2FeSi layer on both the a and c domains of $BaTiO_3$.

The electric field (E) dependence of the low-field MR curves for *device* A and another device (named *device* B) are explored at room temperature in Fig. 6. The data in Fig. 6(a) at $E = 0$ is the same data in Fig. 5(c). Since there are various features in these MR curves, we first focus on the change in the data for *device* A as follows. In Fig. 6(a) we find that the bell-shaped AMR feature gradually disappears with applying E from zero to -1.8 kV/cm. Because the c domains of $BaTiO_3$ are grown by applying E, the uniaxial anisotropy of the Co_2FeSi epilayer on the a domains of $BaTiO_3$ disappears and the cubic magnetocrystalline anisotropy associated with the c domains of $BaTiO_3$ becomes dominant, as confirmed by the M-H curve measurements with applying E [52]. Namely, the MR feature at $E = -1.8$ kV/cm indicates the magnetization reversal process is governed by the Co_2FeSi epilayer on the c domains of $BaTiO_3$. Possible changes in the M direction of the Co_2FeSi epilayer are similar to those shown in Fig. 5(d) ($1 \rightarrow 2 \rightarrow 3 \rightarrow 4$, only on the c domain). From these features, we conclude that, for *device* A, the E effect on the MR curves is governed by the $a - c$ domain wall motion

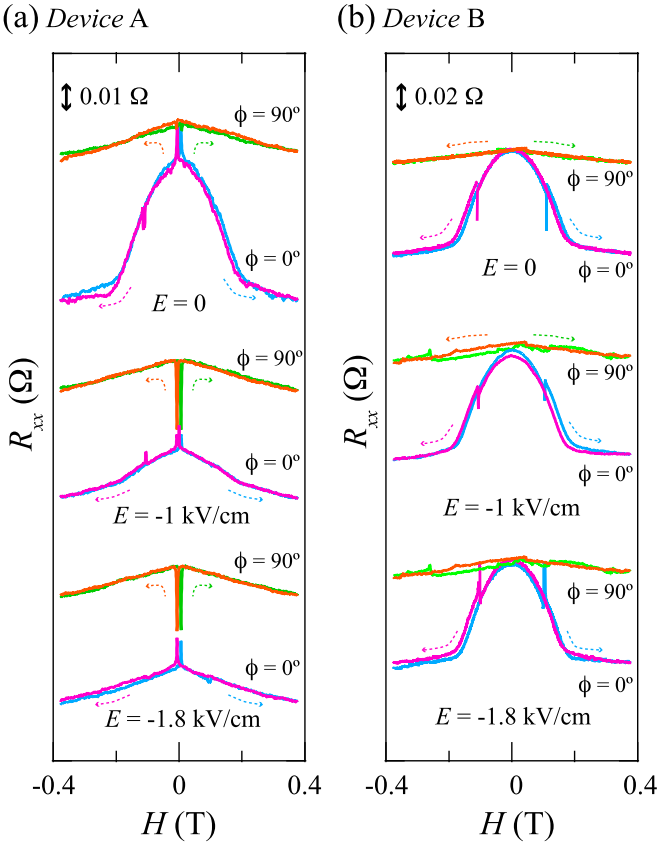

FIG. 6. Low-field MR curves for (a) *device* A and (b) *device* B under various E from zero to -1.8 kV/cm at room temperature. Although there is no difference in the device fabrication process between *device* A and *device* B, the E effect on the MR curves is different.

of $BaTiO_3$. For *device* B, on the other hand, a different feature is seen. Although the bell-shaped curve with respect to H is also observed, similar to those for *device* A, the E effect is not clearly seen within $E \leqslant -1.8$ kV/cm. Notably, we find that there is almost no peak structure from $H \sim -0.006$ T to $H \sim -0.017$ T. The absence of the peak structure means that, for *device* B, the influence of the c domain of $BaTiO_3$ on the magnetization reversal process of the Co_2FeSi epilayer is relatively small compared to that for *device* A. In other words, the $a-c$ domain wall motion of $BaTiO_3$ does not attribute to the magnetization reversal process for *device* B. These facts indicate that the AMR effect allows for high sensitive detection of the difference in the magnetization process in the interfacial multiferroic system.

To clearly show the E effect on the AMR effect, we plot the angular (ϕ) dependence of the AMR ratio for *devices* A and B at room temperature under the application of $H = 0.4$ T in Figs. 7(a) and 7(b), respectively. In this measurement, the AMR ratio (%) is defined as $[(R_\phi - R_{90^\circ})/R_{90^\circ}] \times 100$, where R_ϕ and R_{90° are the resistance at ϕ and 90°, respectively, because a H of 0.4 T is sufficient to saturate the magnetization of the Co_2FeSi layer. As a result, the AMR ratio for *device* A at $E = 0$ is estimated to be -0.073 % [Fig. 7(a)], where the negative value of the AMR ratio indicates that the used Co_2FeSi epilayers have half-metallic nature [53].

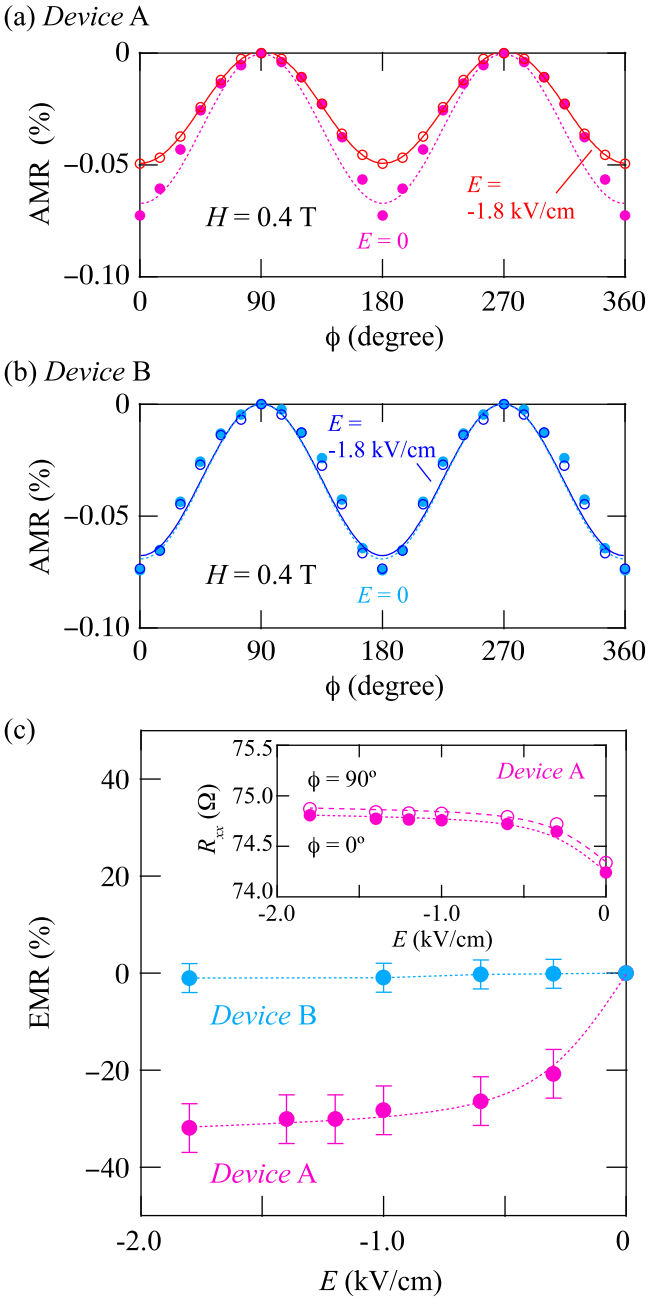

FIG. 7. The angular (ϕ) dependence of the AMR ratio for (a) *device* A and (b) *device* B at $E = 0$ and -1.8 kV/cm at room temperature under $H = 0.4$ T. (c) EMR ratio versus E for *devices* A and B at room temperature. The inset of (c) shows R_{xx} versus E for *device* A under $H = 0.4$ T at $\phi = 0^\circ$ (closed circles) and 90° (open circles), respectively.

By applying $E = -1.8$ kV/cm, the magnitude of the AMR ratio for *device* A is evidently decreased from -0.073% to -0.049%. This means that the AMR ratio can be modulated in the epitaxial $Co_2FeSi/BaTiO_3$ interfacial multiferroic system. For *device* B, on the other hand, it seems that the change in the AMR ratio by applying E is quite small [Fig. 7(b)].

To further understand the E effect on the AMR effect, we summarize the electromagnetoresistance (EMR) ratio as a function of E in Fig. 7(c) for *devices* A and B. The EMR

ratio (%) is defined as $[(MR_E - MR_0)/MR_0] \times 100$ [54,55], where MR_E and MR_0 are the MR values at E and at zero electric field, respectively. For reference, the raw resistance changes with increasing E at $\phi = 0^\circ$ and 90° under $H = 0.4$ T are also shown in the inset. For *device* A, the magnitude of the EMR ratio reaches several tens %. Notably, despite the single ferromagnetic layer, the magnitude of the EMR ratio is relatively large compared to those for Co/Cu/Fe giant magnetoresistance structures [55]. For *device* B, on the other hand, the magnitude of the EMR ratio is relatively small.

Another great advantage is the E controllability of the AMR effect in these interfacial multiferroic system. Because the maximum E value of -1.8 kV/cm is less than the coercive electric field of the used $BaTiO_3$ substrate, the $a - c$ domain wall motion in $BaTiO_3$ is reversibly controlled by tuning E between zero and -1.8 kV/cm. Reflecting the reversible modulation of the domain walls of $BaTiO_3$, the AMR changes for *device* A are also reversible. From these data, the AMR effect is surely tunable by applying E at room temperature fabricated on the a and c domains of $BaTiO_3(001)$.

IV. DISCUSSION

In general, the extrinsic AMR effect can be interpreted in terms of the two-current model [56,57]. When the majority spins (↑) and minority spins (↓) are assumed to constitute two parallel conduction channels with the corresponding resistivities given by $\rho_\uparrow$ and $\rho_\downarrow$, respectively, the AMR ratio can be expressed using $\Delta\rho = (\rho_{//} - \rho_\perp)$ [$\rho_{//}$ and $\rho_\perp$ denote the longitudinal ($M//I$) and transverse ($M\perp I$) resistivity] as follows.

$$\frac{\Delta\rho}{\rho} = \gamma(\alpha - 1), \tag{1}$$

where $\alpha = \frac{\rho_\downarrow}{\rho_\uparrow}$, γ is the constant which is related to the spin-orbit coupling constant λ and exchange interaction energy E_{ex}, i.e., $\gamma = (\frac{\lambda}{E_{ex}})^2$. On the basis of Eq. (1), every material should yield a unique value of the AMR ratio, given λ and E_{ex}. Although the λ and E_{ex} are intrinsic parameters of the material, these are very sensitive to the strain via the interface. Therefore, significant electric field variation of the AMR would occur for FM/FE heterostructures with the salient domain wall motion of FE materials. The description is partly compatible with our experimental data that the E effect on the AMR becomes more significant for *device* A with the $a - c$ domain wall motion in $BaTiO_3$ than *device* B without it.

Since the characteristic length scale of the magnetoelastic effect is beyond several hundreds of nm [13], the long characteristic length indicates that strain-induced magnetoelastic effect can mostly account for the significant E effects on the AMR which appeared in *device* A. In addition to this, other mechanisms cannot be excluded at this stage. To date, there have been some reports on the origin of the E effects on magnetic properties; bonding modulation [20], charge modulation [21], and magnetoionic modulation [22,58], etc, for example. These mechanisms are closely associated with the structural and chemical modulation that leads to a change in E_{ex} in the very vicinity of the interface. The AMR effect we observe in the epitaxial $Co_2FeSi/BaTiO_3$ heterostructures could have the origin same as these effects. We also note that our experimental findings are slightly different from E modulation of the AMR reported in other amorphous or polycrystalline FM/FE multiferroic systems [59,60], where the effects are related to a change in the small magnetic domain structures of FM layers [60]. Although the microscopic origins for the contrasting behavior are not fully understood, the results indicate that the E effects on the AMR we observe arise from a combined effect of possible E modulation of both λ and E_{ex} at the epitaxial interface.

Finally, we should consider the intrinsic mechanism for the AMR effect on the basis of the electronic band structure. Recently, Zeng *et al.* theoretically predicted that the AMR effect of single-crystalline CoFe alloys is strongly related to shifting the special k points near the Fermi level in the band structure by varying alloy composition [61], where the prediction is also experimentally confirmed. If the electric field tunable AMR effect is strongly associated with the epitaxial quality of Co_2FeSi in our interfacial multiferroic heterostructures, we can consider that there is a possible intrinsic mechanism of the tunable AMR effect observed in this study. In the future, we will further examine the correlation between the tunable AMR effect and the variation in the electronic band structure of Co_2FeSi through the domain-wall motion in $BaTiO_3$.

V. CONCLUSION

We have studied magnetic and magnetotransport properties of an interfacial multiferroic system consisting of Co_2FeSi and $BaTiO_3$. For the epitaxial $Co_2FeSi/BaTiO_3$ heterostructures, an in-plane uniaxial magnetic anisotropy and its strong temperature dependence, induced by the presence of the magnetoelastic effect via the spin-orbit interaction at the epitaxial $Co_2FeSi/BaTiO_3(001)$ interface, have been observed. Also, in Co_2FeSi Hall-bar devices, the AMR hysteretic curves depending on the in-plane magnetization reversal processes on the a and c domains of $BaTiO_3(001)$ were clearly observed at room temperature. Notably, the magnitude of the AMR ratio (%) for Co_2FeSi Hall-bar devices can be tuned through the $a - c$ domain wall motion of $BaTiO_3(001)$ by applying electric fields. We propose that the electric field tunable AMR effect is associated with the modulation of the spin-orbit interaction, exchange interaction, and/or the electronic band structure near the Fermi level by applying electric fields in the epitaxial $Co_2FeSi/BaTiO_3(001)$ interfacial multiferroic system.

ACKNOWLEDGMENTS

This work was partly supported by JST CREST Grant No. JPMJCR18J1, JSPS KAKENHI Grants No. 18KK0111, No. 17H03377, and No. 18F18353 and research grants from the Mazda Foundation (J191103163), the Asahi Glass Foundation, and the Kato Foundation for Promotion of Science. The SuperSTEM Laboratory is the UK National Research Facility for Aberration-Corrected STEMAdvanced Electron Microscopy, supported by the Engineering and Physical Sciences Research Council (EPSRC).

[1] H. Ohno, D. Chiba, F. Matsukura, T. Omiya, E. Abe, T. Dietl, Y. Ohno, and K. Ohtani, Nature (London) **408**, 944 (2000).

[2] M. Weisheit, S. Fähler, A. Marty, Y. Souche, C. Poinsignon, and D. Givord, Science **315**, 349 (2007).

[3] T. Maruyama, Y. Shiota, T. Nozaki, K. Ohta, N. Toda, M. Mizuguchi, A. A. Tulapurkar, T. Shinjo, M. Shiraishi, S. Mizukami, Y. Ando, and Y. Suzuki, Nat. Nanotechnol. **4**, 158 (2009).

[4] D. Chiba, S. Fukami, K. Shimamura, N. Ishiwata, K. Kobayashi, and T. Ono, Nat. Mater. **10**, 853 (2011).

[5] T. Kimura, T. Goto, H. Shintani, K. Ishizaka, T. Arima, and Y. Tokura, Nature (London) **426**, 55 (2003).

[6] W. Eerenstein, N. D. Mathur, and J. F. Scott, Nature (London) **442**, 759 (2006).

[7] J. P. Velev, S. S. Jaswal, and E. Y. Tsymbal, Phil. Trans. R. Soc. A **369**, 3069 (2011).

[8] J.-M. Hu, Z. Li, L.-Q. Chen, and C.-W. Nan, Nat. Commun. **2**, 553 (2011).

[9] S. Zhang, Y. G. Zhao, P. S. Li, J. J. Yang, S. Rizwan, J. X. Zhang, J. Seidel, T. L. Qu, Y. J. Yang, Z. L. Luo, Q. He, T. Zou, Q. P. Chen, J. W. Wang, L. F. Yang, Y. Sun, Y. Z. Wu, X. Xiao, X. F. Jin, J. Huang, C. Gao, X. F. Han, and R. Ramesh, Phys. Rev. Lett. **108**, 137203 (2012).

[10] J. T. Heron, J. L. Bosse, Q. He, Y. Gao, M. Trassin, L. Ye, J. D. Clarkson, C. Wang, J. Liu, S. Salahuddin, D. C. Ralph, D. G. Schlom, J. Íñiguez, B. D. Huey, and R. Ramesh, Nature (London) **516**, 370 (2014).

[11] Y. Shirahata, R. Shiina, D. L. González, K. J. A. Franke, E. Wada, M. Itoh, N. A. Pertsev, S. van Dijken, and T. Taniyama, NPG Asia Mater. **7**, e198 (2015).

[12] T. Taniyama, J. Phys.: Condens. Matter **27**, 504001 (2015).

[13] J.-M. Hu, L.-Q. Chen, and C.-W. Nan, Adv. Mater. **28**, 15 (2016).

[14] A. E. Bocirnea, D. G. Popescu, C. Chirila, R. M. Costescu, V. Kuncser, V. Stancu, L. Trupina, I. Pasuk, A. M. Vlaicu, and M. A. Husanu, Phys. Rev. Materials **4**, 034402 (2020).

[15] S. Sahoo, S. Polisetty, C.-G. Duan, S. S. Jaswal, E. Y. Tsymbal, and C. Binek, Phys. Rev. B **76**, 092108 (2007).

[16] T. Taniyama, K. Akasaka, D. Fu, and M. Itoh, J. Appl. Phys. **105**, 07D901 (2009).

[17] Y. Shirahata, T. Nozaki, G. Venkataiah, H. Taniguchi, M. Itoh, and T. Taniyama, Appl. Phys. Lett. **99**, 022501 (2011).

[18] T. H. E. Lahtinen, K. J. A. Franke, and S. van Dijken, Sci. Rep. **2**, 258 (2012).

[19] R. Lo Conte, J. Gorchon, A. Mougin, C. H. A. Lambert, A. El-Ghazaly, A. Scholl, S. Salahuddin, and J. Bokor, Phys. Rev. Materials **2**, 091402(R) (2018).

[20] C.-G. Duan, S. S. Jaswal, and E. Y. Tsymbal, Phys. Rev. Lett. **97**, 047201 (2006).

[21] C. A. F. Vaz, J. Hoffman, Y. Segal, J. W. Reiner, R. D. Grober, Z. Zhang, C. H. Ahn, and F. J. Walker, Phys. Rev. Lett. **104**, 127202 (2010).

[22] U. Bauer, L. Yao, A. J. Tan, P. Agrawal, S. Emori, H. L. Tuller, S. van Dijken, and G. S. D. Beach, Nat. Mater. **14**, 174 (2015).

[23] K. Yamauchi, B. Sanyal, and S. Picozzi, Appl. Phys. Lett. **91**, 062506 (2007).

[24] L. Y. Chen, C. L. Chen, K. X. Jin, and X. J. Du, Europhys. Lett. **99**, 57008 (2012).

[25] V. Gunawan and R. L. Stamps, Phys. Rev. B **85**, 104411 (2012).

[26] J. Chen, C. Lin, Y. Yang, L. Hu, and W. Cheng, Modelling Simul. Mater. Sci. Eng. **22**, 015008 (2014).

[27] L. Yu, G. Gao, L. Zhu, L. Deng, Z. Yang, and K. Yao, Phys. Chem. Chem. Phys. **17**, 14986 (2015).

[28] I. Galanakis, P. H. Dederichs, and N. Papanikolaou, Phys. Rev. B **66**, 174429 (2002).

[29] K. Inomata, N. Ikeda, N. Tezuka, R. Goto, S. Sugimoto, M. Wojcik, and E. Jedryka, Sci. Technol. Adv. Mater. **9**, 014101 (2008).

[30] C. Felser, L. Wollmann, S. Chadov, G. H. Fecher, and S. S. P. Parkin, APL Mater. **3**, 041518 (2015).

[31] Y. Sakuraba, M. Hattori, M. Oogane, Y. Ando, H. Kato, A. Sakuma, T. Miyazaki, and H. Kubota, Appl. Phys. Lett. **88**, 192508 (2006).

[32] M. Yamamoto, T. Ishikawa, T. Taira, G.-F. Li, K. Matsuda, and T. Uemura, J. Phys.: Condens. Matter **22**, 164212 (2010).

[33] K. Hamaya, N. Hashimoto, S. Oki, S. Yamada, M. Miyao, and T. Kimura, Phys. Rev. B **85**, 100404(R) (2012).

[34] R. Farshchi and M. Ramsteiner, J. Appl. Phys. **113**, 191101 (2013).

[35] T. A. Peterson, S. J. Patel, C. C. Geppert, K. D. Christie, A. Rath, D. Pennachio, M. E. Flatté, P. M. Voyles, C. J. Palmstrøm, and P. A. Crowell, Phys. Rev. B **94**, 235309 (2016).

[36] Y. Fujita, M. Yamada, M. Tsukahara, T. Oka, S. Yamada, T. Kanashima, K. Sawano, and K. Hamaya, Phys. Rev. Appl. **8**, 014007 (2017).

[37] S. Yamada, K. Hamaya, K. Yamamoto, T. Murakami, K. Mibu, and M. Miyao, Appl. Phys. Lett. **96**, 082511 (2010).

[38] S. Yamada, K. Tanikawa, S. Oki, M. Kawano, M. Miyao, and K. Hamaya, Appl. Phys. Lett. **105**, 071601 (2014).

[39] K. Kudo, Y. Hamazaki, S. Yamada, S. Abo, Y. Gohda, and K. Hamaya, ACS Appl. Electron. Mater. **1**, 2371 (2019).

[40] S. Wurmehl, G. H. Fecher, H. C. Kandpal, V. Ksenofontov, C. Felser, H.-J. Lin, and J. Morais, Phys. Rev. B **72**, 184434 (2005).

[41] B. Balke, G. H. Fecher, H. C. Kandpal, C. Felser, K. Kobayashi, E. Ikenaga, J.-J. Kim, and S. Ueda, Phys. Rev. B **74**, 104405 (2006).

[42] K. Hamaya, T. Taniyama, Y. Kitamoto, R. Moriya, and H. Munekata, J. Appl. Phys. **94**, 7657 (2003).

[43] H. F. Kay and P. Vousden, Philos. Mag. **40**, 1019 (1949).

[44] T. Kimura, N. Hashimoto, S. Yamada, M. Miyao, and K. Hamaya, NPG Asia Mater. **4**, e9 (2012).

[45] K. Hamaya, T. Kurokawa, S. Oki, S. Yamada, T. Kanashima, and T. Taniyama, Phys. Rev. B **94**, 140401(R) (2016).

[46] W. J. Merz, Phys. Rev. **95**, 690 (1954).

[47] G. Arlt and P. Sasko, J. Appl. Phys. **51**, 4956 (1980).

[48] Y. Yoneda, Y. Kohmura, Y. Suzuki, S. Hamazaki, and M. Takashige, J. Phys. Soc. Jpn. **73**, 1050 (2004).

[49] See Supplemental Material at http://link.aps.org/supplemental/10.1103/PhysRevMaterials.5.014412 for $M - H$ curves for a 5-nm-thick Co_2FeSi epilayer on $BaTiO_3(001)$.

[50] R. P. Cowburn, S. J. Grey, J. Ferré, J. A. C. Bland, and J. Miltat, J. Appl. Phys. **78**, 7210 (1995).

[51] U. Welp, V. K. Vlasko-Vlasov, X. Liu, J. K. Furdyna, and T. Wojtowicz, Phys. Rev. Lett. **90**, 167206 (2003).

[52] S. Hu, S. Yamada, P. Chang, W. Lin, K. Hamaya, and T. Kimura (unpublished).
[53] Y. Sakuraba, S. Kokado, Y. Hirayama, T. Furubayashi, H. Sukegawa, S. Li, Y. K. Takahashi, and K. Hono, Appl. Phys. Lett. **104**, 172407 (2014).
[54] L. Bocher, A. Gloter, A. Crassous, V. Garcia, K. March, A. Zobelli, S. Valencia, S. Enouz-Vedrenne, X. Moya, N. D. Marthur, C. Deranlot, S. Fusil, K. Bouzehouane, M. Bibes, A. Barthélémy, C. Colliex, and O. Stéphan, Nano Lett. **12**, 376 (2012).
[55] S. S. Pillai, H. Kojima, M. Itoh, and T. Taniyama, Appl. Phys. Lett. **107**, 072903 (2015).
[56] O. Jaoul, I. A. Campbell, and A. Fert, J. Magn. Magn. Mater. **5**, 23 (1977).
[57] A. P. Malozemoff, Phys. Rev. B **34**, 1853 (1986).
[58] C. Leighton, Nat. Mater. **18**, 13 (2019).
[59] M. Liu, S. Li, O. Obi, J. Lou, S. Rand, and N. X. Sun, Appl. Phys. Lett. **98**, 222509 (2011).
[60] W. Zhou, C. Ma, C. Gan, Z. Zhang, X. Wang, W. Tan, and D. Wang, Appl. Phys. Lett. **111**, 052401 (2017).
[61] F. L. Zeng, Z. Y. Ren, Y. Li, J. Y. Zeng, M. W. Jia, J. Miao, A. Hoffmann, W. Zhang, Y. Z. Wu, and Z. Yuan, Phys. Rev. Lett. **125**, 097201 (2020).